Numerical Calculation of 3D Low Speed Delta Wing Fighters Jet Aircraft

Haci Sogukpinar
Department of Electric and Energy,
Vocational School, University of Adiyaman,
Adiyaman 02040, Turkey, hsogukpinar@adiyaman.edu.tr

ABSTRACT

In this study, numerical calculations are conducted to investigate aerodynamic characteristics of the delta wing 3D fighter jet aircraft at low speed. Since the NACA 64A204 and 63A203 airfoil data are not available in the literature therefore 64A210 airfoil data are taken as a reference for estimation. The fuselage of the aircraft is created with 64A204 airfoil, and for the wings 64A204 and 64A203 airfoils are used. Numerical calculations are performed for estimated 2D airfoils and lift coefficient are calculated and compared with other numerical study. Numerical simulations are then conducted for 3D model by varying angle of attack to investigate wing tip vortexes by using SST turbulence model. 3D model aircraft are simulated for cruise flight, climb and descent at the angle of attack +10° and -10° respectively. The simulation results are interpreted in terms of fluid dynamics. A huge vortex covering the entire plane is simulated during the climb and descent. Numerical calculation results show that vortexes direction changed in climb and descent. The vortex rolls up and continues to curl inward at the angle of attack +10° and roll down during negative angle of attack.

KEYWORDS : *3D simulation, Aircraft, vortex, airfoil, Aerodynamic Analysis, lift, drag*

NOMENCLATURE

c_P	Pressure coefficient
c_L	Lift coefficient
f_{w1}	Damping fuction
P	Static pressure
P_∞	Free stream pressure
U_r	Relative velocity
U_∞	Free stream velocity (wind velocity)
v	Kinematic viscosity
c	Airfoil chord
t	Percentage of the maximum thickness
k	Turbulence kinetic energy
κ	Von Kármán constant,
l_{ref}	Reference length scale
L	Length scale of flow
ε	Turbulence dissipation rate
ω	Specific dissipation rate
ω_t	Wall vorticity at the trip
ρ	Density
ρ_∞	Freestream density
μ	Dynamic viscosity
S	magnitude of the vorticity,
$\tilde{S}$	Modified vorticity
S_{ij}	Mean strain rate
Ω_{ij}	Mean rotation rate
μ_{eff}	Effective dynamic viscosity
α	Angle of attack
∅	Scalar quantity of the flow
CFD	Computational fluid dynamics
DES	Detached-Eddy Simulation
NACA	National Advisory Committee for Aeronautics
NASA	National Aeronautics and Space Administration
RANS	Reynolds Averaged Navier Stokes equations
SST	Shear Stress Transport

1 PAPER CONTENT

1.1. Introduction

Today with the development of high-quality computer, computational fluid dynamics (CFD) has taken the complementary position to wind tunnel and flight test. In this way, the CFD methods shorten preliminary design times and provide economic advantages as well. Thirty to forty years ago only the analytical methods were used before the flight and wind tunnel tests, but nowadays, computational fluid dynamics have taken the first stage in design process.

In order to complete the design of an aircraft at Boeing Commercial Airplanes Company, more than 20,000 CFD cases were run before completion [1]. For instance, examples which is part of the design that it is not possible to test in the wind tunnel or it may be dangerous to carry out the flight test; on these drums only the CFD method is used to investigate aerodynamic behaviors [2]. Prior to the application of such CFD methods, they should be evaluated against wind tunnel and test flight. Another issue that effect accuracy of simulation is proper choice of the physical model used. Employing too simple or too complex physical model affects computational results. Mathematical definition of the flow physics is provided by Navier-Stokes equations. Different models were developed like SST (Shear Stress Transport), k-w, Spalart–Allmaras to simulate the turbulence flow depending on the Reynolds Average Navier-Stokes (RANS) equations. CFD calculations along the X-31 aircraft were conducted at the high angle of attack by using k-w turbulence model and obtained data were compared with wind tunnel test. Results provide an excellent data set for verification and evaluation [2]. Comparison of measured and Block Structured Simulation were performed for F-16XL aircraft by using three RANS model of k–e, k–w and Algebraic Stress turbulence model for the feature of vertical flow [3]. The agreement between numerical approaches and the flight test data is very good. Detached-Eddy Simulation (DES) was conducted for the F-15E at the angle of attack 65° with Reynold numbers of 13.6×10^6 and Mach number of 0.3. [4] DES method simulates based on modification of Spalart–Allmaras model and reduces RANS formulation near solid surfaces and away from wall to a sub-grid model [5, 6]. The lift, drag and pitching moments predicted from both RANS and DES shows good agreement with the Boeing database but DES shows slightly better predictions. 3D flow calculation over a realistic aircraft was conducted to validate simulation integrity of the Computational Fluid Dynamics using an unstructured mesh method [7]. High-lift configuration with a nacelle-pylon was simulated by Spalart–Allmaras turbulence model without trip term and compared with experimental data. CFD calculation result indicates that there is a good agreement including the local flow. Numerical simulation was performed to investigate Wing-Body Stage flow separation by using Navier-Stokes and Cartesian grid Euler equation at the Mach numbers of 2 to 6 [8]. A good agreement was observed between Navier-Stokes, Euler and wind tunnel results in steady state. CFD is now accepted to provide significant value and has created a paradigm shift in vehicle design, analysis and support processes [1] and has joined the wind tunnel and flight test as primary tools of the trade [9].

It is rarely seen that a whole plane is simulated and a three-dimensional velocity graph around airplane is plotted. However, three dimensional turbulence flow image in real flight tests are available. Therefore in this study, to see the harmony between the theoretical calculation and the experiment, a fighter jet is designed and modeled in computer environment and numerical calculation is carried out by using SST turbulence model at the airflow velocity of 10 m/s, and obtained results compared with real flight test. The resulting waves, vortices are interpreted and visually presented in figures.

1.2. SST Turbulence Model Methodology

A Reynolds-Averaged Navier–Stokes (RANS) equation with Menter's Shear Stress Transport (SST) turbulence model is a widely used as robust two-equation eddy-viscosity turbulence model in Computational Fluid Dynamics (CFD). SST turbulence model combines the superior behavior of the k-ω model in the near-wall region with the robustness of the k-ε model [10]. To achieve this, the k-ε model is converted into a k-ω formulation but it contains some improvements [11]. The model equations are represented in terms k and ω with the Eq.1 and Eq.2.

$$\rho\frac{\partial k}{\partial t}+\rho u.\nabla k=P-\rho{\beta_0}^{*}k\omega+\nabla.((\mu+\sigma_k\mu_T)\nabla_k) \tag{1}$$

$$\rho\frac{\partial \omega}{\partial t}+\rho u.\nabla \omega=\frac{\rho\gamma}{\mu_T}P-\rho\beta\omega^2+\nabla.\left((\mu+\sigma_\omega\mu_T)\nabla_\omega\right)+2(1-f_{v1})\frac{\rho\sigma_{\omega^2}}{\omega}\nabla\omega.\nabla k \tag{2}$$

Where, ρ is density, u is velocity field of wind, k is turbulent kinetic energy, μ is dynamic viscosity of air, ω is specific dissipation rate, ${\beta_0}^{*}$, σ_k, β, σ_ω are turbulence model parameters.
A production limiter is used in the SST model to prevent turbulence formation in stagnation zones.

$$\check{P}=\min(P_k,10\rho{\beta_0}^{*}k\omega) \tag{3}$$

Where, P_k is production term and expressed by Eq.4:

$$P_k = \mu_T\left(\nabla u:(\nabla u + (\nabla u)^T) - \frac{2}{3}(\nabla . u)^2\right) - \frac{2}{3}\rho k \nabla . u \tag{4}$$

Where, $\mu_T$is turbulence eddy viscosity and expressed by Eq.5:

$$\mu_T = \frac{\rho a_1 k}{\max(a_1 \omega, S f_{v2})} \tag{5}$$

Where, S is the constant measure of the strain rate, f_{v1} and f_{v2} are first and second blending functions [12] respectively, and are defined by Eq.6 and Eq.7.

$$f_{v1} = \tanh\left(min\left[max\left(\frac{\sqrt{k}}{\beta_0{}^* \omega l_\omega}, \frac{500\mu}{\rho \omega l_\omega{}^2}\right), \frac{4\rho\sigma_\omega{}_2 k}{\max(\frac{2\rho\sigma_\omega 2}{\omega}\nabla\omega . \nabla k, 10^{-10}) l_\omega{}^2}\right]^4\right) \tag{6}$$

$$f_{v2} = tanh\left(max\left(\frac{\sqrt{k}}{\beta_0{}^* \omega l_\omega}, \frac{500\mu}{\rho \omega l_\omega{}^2}\right)^2\right) \tag{7}$$

According to the k-ε model, f_{v1} is equal to zero away from the surface but in k-ω model that switches over to the inside of the boundary layer. l_ω is the distance to the closest wall and these blending functions include an explicit measurement of the wall distance. The default constants for this model are given by:

$\beta_1 = 0.075, \gamma_1 = \frac{5}{9}, \sigma_{k1} = 0.85, \sigma_{\omega 1} = 0.5, \beta_2 = 0.0828, \gamma_2 = 0.44, \sigma_{k2} = 1.0, \sigma_{w2} = 0.856, \beta_0{}^* = 0.09, \sigma_1 = 0.31.$ Reynolds Average Navier-Stokes (RANS) equations are solved for conservation of momentum and continuity equation for conservation of mass. Turbulence effects are modeled using two of Shear Stress Transport (SST) Eq.1 and Eq.2. The SST model is also called the Low Reynolds Number Model and flows are solved all the way to the wall by using wall distance equation. The inlet port is set to velocity inlet and outlet port is set to pressure outlet with zero atmospheric pressure. Inlet velocity is decided as normal inflow velocity of 10 m/s. No slip boundary condition is applied for the model surface. The commercial software COMSOL, based on finite volume method is applied. An airfoil with max thickness 4% at 40% chord and max camber 1% at 40% chord which is similar to the real NACA 64A204 is created by using the 64A210 airfoil data as reference. Closed-up of the newly created airfoil is given in Fig. 1.

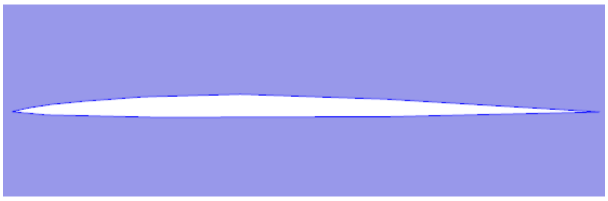

Figure 1. Close up of airfoil section.

The full designed model aircraft is given in Fig. 2.

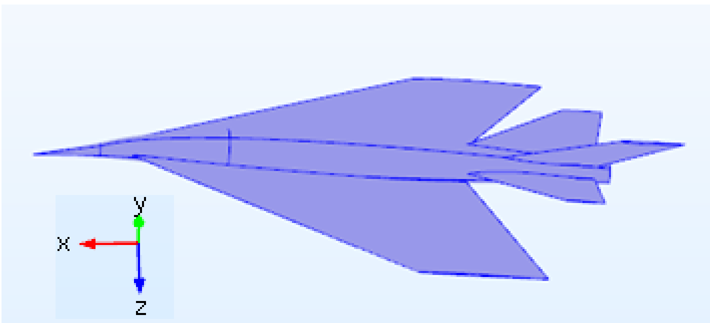

Figure 2. Model aircraft

Model consists of 16 domain and tetrahedral mesh type is applied. Model plane is splitted into 718356 mesh elements. An intense mesh distribution is applied to the outer surface portion of the model and mesh distribution is given in Fig.3.

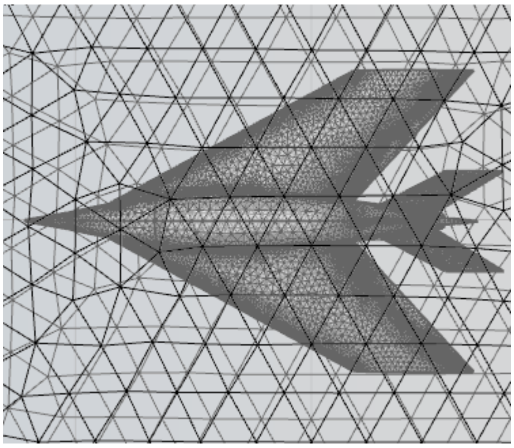

Figure 3. Mesh distribution around the model

1.3. Results and Discussions

Since NACA 64A204 and 64A203 airfoil data are not found in the literature, so these two airfoil data are estimated by using NACA 64A210 data, which is thought to be the most similar to these airfoils. Previously, numerical calculation is performed for NACA 64A210 airfoil using SST turbulence model and the obtained data are compared with those obtained other calculation in Ref. [13] to validate simulation accuracy of this calculation. Lift coefficient with respect to angle of attack for NACA 64A210 is shown in Fig.4. The comparison between this calculation and previous one show good agreement and results are found to be very well matched for NACA 64A210. Therefore, numerical approaches are reliable to investigate aerodynamic performance of other airfoil in this study. 64A204 and 64A203 are simulated by using SST turbulence model and lift coefficient are calculated and presented in the same Fig.4 together with NACA 64A210 airfoil data. The maximum lift coefficient is calculated at around 6° to 7° for both airfoils, and lift coefficient began to decrease with the increasing angle of attack further than 7°. Geometric and computer analysis of the F-35A Lightning II airfoil of 64A206 was reported at the Ref. [14] and maximum lift coefficient calculated as 0.62 at the angle of attack around 9°. Although airfoils used in this study are slender, the maximum lift coefficient is calculated as 0.6 at the angle of attack around 7°. The maximum lift coefficient angle is lower than NACA 64A206 because 64A210 airfoil airfoil is thinner.

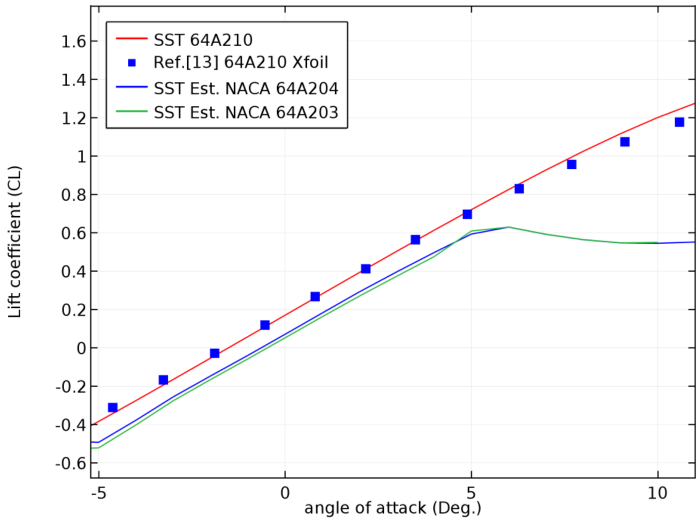

Figure 4. 2D computational results for the lift coefficient vs. angle of attack.

The model aircraft's fuselage is designed with NACA 64A204, and for the other part 64A204 and 64A203 airfoils are used. 10° anhedral angle is set to wing so wing tip is lower than x-y plane. Angle between the fuselage center line and wing chord line is set to zero degree. Numerical calculation is conducted at the Reynolds numbers of $1x10^6$ and inlet wind speed set to 10 m/s. In all calculations, the fluid is sent from the front to the back side (+x to –x) of the airplane. The distance between the streamlines is taken quite short to prevent mixing streamlines and also for the clear view of the vortex directions. The bottom and top views of streamline simulation result of the plane for the cruise flight are given in Fig.5(a) and Fig.5(b).Streamlines goes from left to right and figure shows that the airflow velocity on the surface of the body is reduced due to the no slip condition. There is also a wake zone in the back of the aircraft where the shedding effect dominates, and low speed region extended further more.

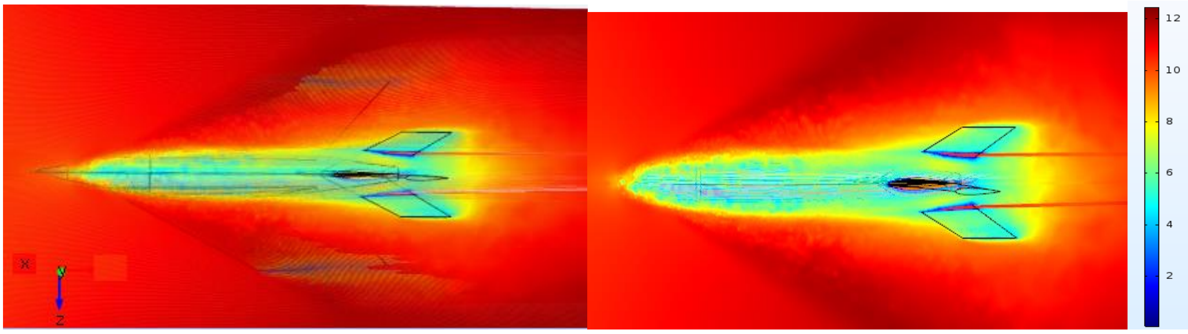

Figure 5. Velocity (m/s) streamlines of bottom (a) and top view (b) of the plane during a straight flight

For the numerical calculation, airflow is sent over x-y plane along the fuselage center line at cruise flight and calculation data for velocity streamline for upper rear side view of model aircraft is given in Fig.6. Vortex is observed in places where the fluid interacts with the wing then wave rolls up and then continue to curl inward. Negative dihedral angle appears to increase vortex formation as seen in the Fig.6. A lower dihedral angle can be set to increase the lift or to reduce the drag coefficient but for spiral stability negative dihedral angle is necessary for fighter jet. Positive dihedral angle also acts in the direction of increasing vortex formation but positive dihedral angle is set to transport aircraft to adjust lateral stability. Depending on the operational requirement, a positive or negative dihedral angle may be set, but it should be noted that the more laterally stable aircraft means less rolling controllable.

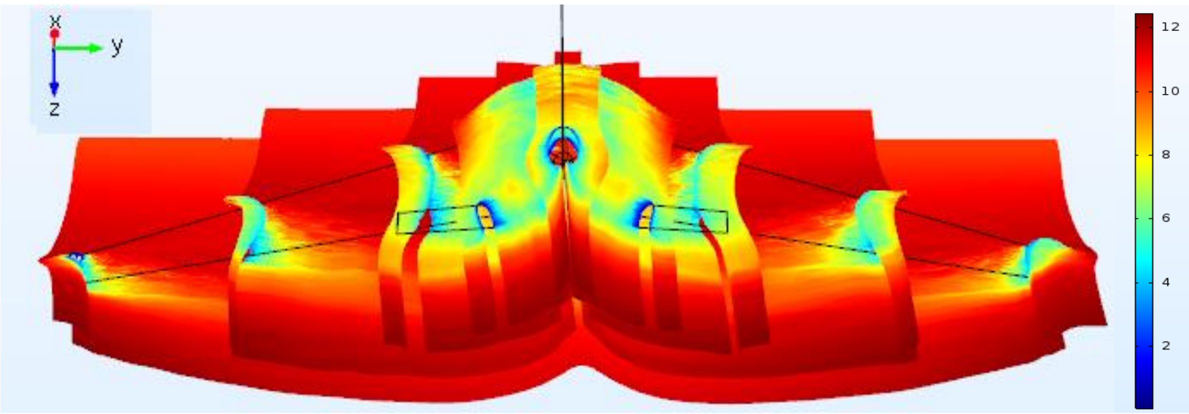

Figure 6. Velocity (m/s) streamlines of upper rear side view of cruise flight

The upper rear views of the wing tip vortex, covering the entire surface of the aircraft ascending with the angle of attack 10°, is given in Fig.7. For this part, fluid is sent over the x-y plane along the fuselage centerline (+x to –x direction) as two layers, first one is passing over the top and second one is along the bottom surface. In rectangular or trapezoid wings, it is known that the vortex occurs only at the wing tip, but it appears that the vortex formation covers the entire aircraft in delta wings as shown in Fig. 7. NASA conducted experimental test to investigate wing vortices for C-5A wings at NASA Langley Research Center [15]. The test was carried out using colored gases spraying at different heights over the mast from ground during low level flight. Experimental test shows that the vortex waves were observed to roll up the whole body bilaterally. A video was recorded during take-off by Alessandra Otondo, a large spiral vortex covers half of the plane and it is available in Ref. [16]. The numerical results obtained in this study are consistent with the experimental data given in the Ref. [15] and Ref. [16].

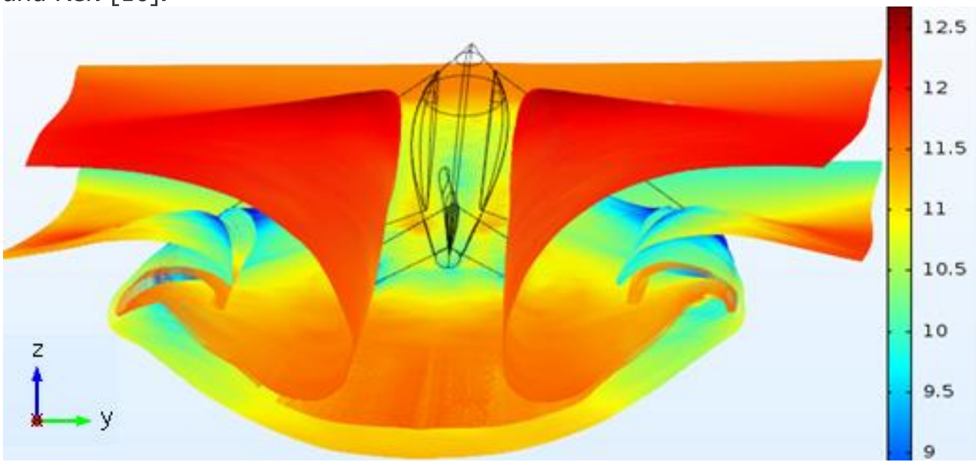

Figure 7. The rear upper side view of velocity (m/s) streamline of plane, ascending at 10° angle of attack.

Upper rear view of streamline velocity of the wing tip vortex, covering the entire surface of the aircraft descending with the angle of attack -10°, is given in Fig.8. During positive angle of attack, wave rolls up and continue to curl inward behind the plane but when the plane is inclined downward with the angle of attack -10°, the vortex is formed in the reverse direction as shown in Fig.8. This is due to the low pressure happening in the rear upper or rear lower part of the aircraft. When the plane is inclined upwards, low pressure occurs at the rear upper part of the aircraft and the fluid is curled and moved to this part. However when the plane is inclined downward, low pressure occurs at the rear lower part of the aircraft and the fluid is curled toward this side.

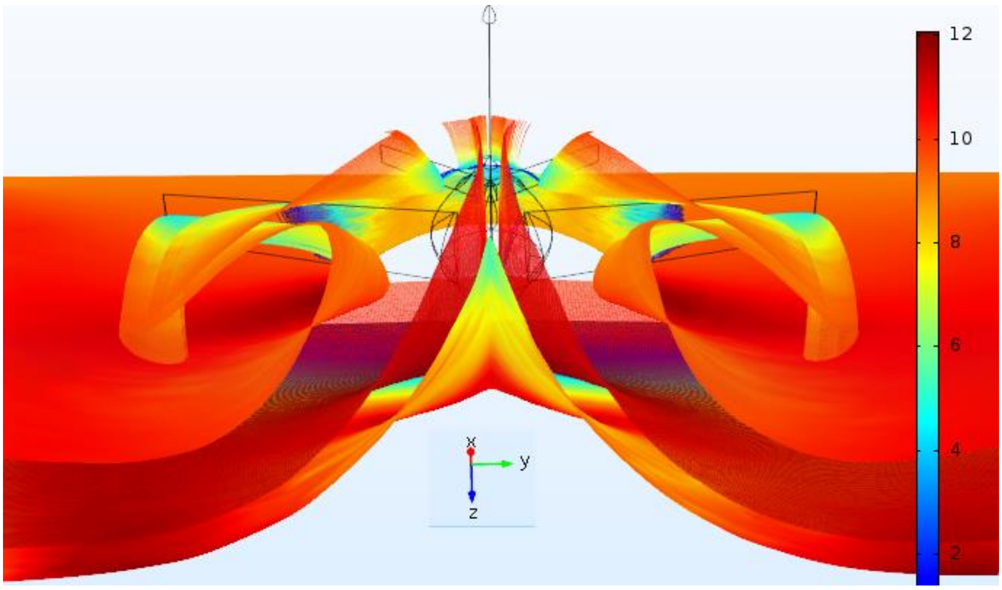

Figure 8. The upper rear view of velocity (m/s) streamline of plane descending at -10° angle of attack

Side views of velocity (m/s) streamline of the aircraft ascending and descending at the angle of attack 10° are given in Fig.9(a) and Fig.9(b) respectively. In Fig.9(a), the airplane is tilted upward by +10 degrees and the airflow is sent on x-y plane over the tip of the aircraft's nose from +x to -x direction. Calculation results show that the fluid bends down to the plane surface as it goes to the back side. This is because a low pressure region is formed on the rear upper surface of the aircraft. As shown in Fig.9(b), airflow is sent beneath the tip of the nose from +x to -x direction on the x-y plane. In this case fluid bends upper side as it goes to the back. This is because a low pressure region is formed on the rear lower surface of the aircraft.

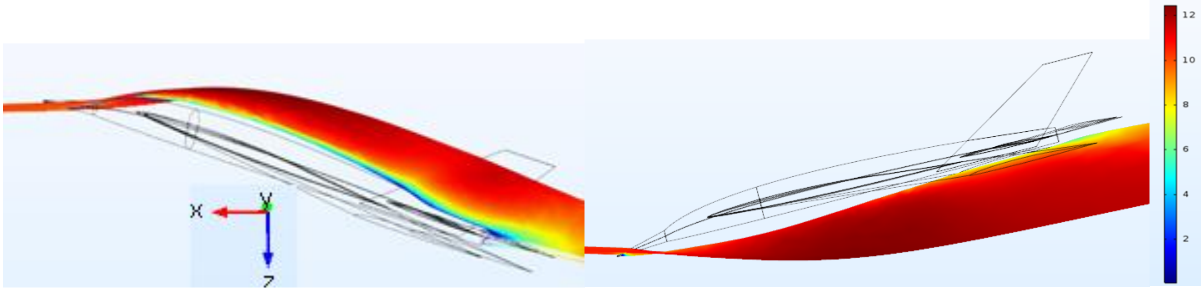

Figure 9. Side view of velocity (m/s) streamline of the plane ascending (a) and descending (b) at 10 degree angle of attack.

1.4. Conclusion

In this study, the interaction of the fluid with the whole aircraft is numerically investigated by using SST turbulence model. Initially, numerical calculations are performed for NACA 64A210 airfoil and obtained data are compared with other numerical data to validate simulation accuracy of this calculation. The comparison shows good agreement for numerical approaches. Then, 64A203 and 64A204 airfoils are estimated by using 64A210 airfoil's data as reference. 64A203 and 64A204 airfoils are simulated and compared with those obtained from other numerical study conducted for NACA 64A210 airfoil. The comparison shows good agreement for the lift coefficient at the angle of attack from -5° to +6 degree. With the increasing angle of attack, the lift coefficient increases in parallel with the reference airfoil but it starts to decrease starting from 6°. The fuselage of jet aircraft is created from 64A204 airfoil, and for the wings, both 64A203 and 64A204 airfoils are used. Next, the whole aircraft is simulated and aerodynamic performance is investigated for cruise flight, climb and descent at the angle of attack +10° and -10° respectively by using SST turbulence model. As the plane tilted up or down, wingtip vortex is observed to covers the whole aircraft. While the plane is ascending at the positive angle of attack (+10°), it rolls up and continues to curl inward along the lateral wing surface, and when the plane is descending at negative angle of attack (-10°), circular wave rolls down outward from the lateral surface. Numerical calculation shows that this is caused by the pressure difference between the front and rear side of the airplane. When the plane is inclined upwards, low pressure is created at the top back of the airplane; while the plane was inclined downward, low pressure is created at the lower back side of the airplane.

ACKNOWLEDGMENT

Many thanks to Middle East Technical University and Adiyaman University for technical support.

REFERENCES

1. T. J. Forrester, E. N. Tinoco, N. J. Yu; 2005; "Thirty years of development and application of CFD at Boeing Commercial Airplanes"; Computers & Fluids; 34;pp. 1115–1151.
2. O.J. Boelens; 2012; "CFD analysis of the flow around the X-31 aircraft at high angle of attack"; Aerospace Science and Technology; 20; pp. 38–51.
3. O. J. Boelens; 2009; "Comparison of measured and block structured simulation results for the F-16XL aircraft." Journal of Aircraft; 46(2); pp. 377-384.
4. J. R. Forsythe, K. D. Squires, K. E. Wurtzler, and P. R. Spalart; 2004; "Detached-Eddy Simulation of the F-15E at High Alpha"; Journal of Aircraft; Vol. 41; No. 2; pp. 193-200.
5. P. R. Spalart, S. R. Allmaras; 1994; "A One-Equation Turbulence Model for Aerodynamic Flows" La Recherche Aerospatiale; No. 1; pp. 5–21.

6. P. R. Spalart; 2000; “Strategies for Turbulence Modeling and Simulations”; International Journal of Heat and Fluid Flow; Vol. 21; pp. 252–263.
7. M. Murayama, Y. Yokokawa, K. Yamamoto, and Y. Ueda; 2007; "CFD Validation Study for a High-Lift Configuration of a Civil Aircraft Model"; 25th AIAA Applied Aerodynamics Conference; June 25 - 28, Miami, FL; pp. 1-20.
8. P.G. Buning, , R. J. Gomez, and W. I. Scallion; 2004; "CFD approaches for simulation of wing-body stage separation"; 22nd Applied Aerodynamics Conference and Exhibit; August 16 - 19, Providence, Rhode Island; pp.1-11.
9. E.N Tinoco; 1998; ”The changing role of computational fluid dynamics in aircraft development”; 16th AIAA Applied Aerodynamics Conference, Fluid Dynamics and Co-located Conferences; Albuquerque, NM; June 15-18; pp.161-174.
10. F.R. Menter; 1994; “Two-Equation Eddy-Viscosity Turbulence Models for Engineering Applications,” AIAA Journal; vol. 32; no. 8;
11. D. C. Eleni, I. T. Athanasios and M. P. Dionissios; 2012; “Evaluation of the turbulence models for the simulation of the flow over a National Advisory Committee for Aeronautics (NACA) 0012 airfoil” Journal of Mechanical Engineering Research; Vol. 4(3); pp. 100-111.
12. F. R. Menter, M. Kuntz, and R. Langtry; 2003; "Ten years of industrial experience with the SST turbulence model"; Turbulence, heat and mass transfer 4; 4(1); pp.625-632.
13. “Airfoil database search”; 2017; http://airfoiltools.com/.
14. A.Bhatt, M. Harvey, R. Hofmeister; 2017; “Computer and Geometrical Analysis of the F-35A Lightning II”; www.dept.aoe.vt.edu.
15. M.Curry; 2017;“C-5A Wing Vortice tests at NASA Langley Research Center”; https://www.dfrc.nasa.gov
16. T. Cookers; 2017; “Wingtip Vortices”; http://www.f1technical.net